

# Homostructure and Heterostructure Photonic Crystals based on VCSEL Arrays

D.L. Boiko, G. Guerrero, E. Kapon

Laboratory of Physics of Nanostructures

Institute of Quantum Electronics and Photonics, Swiss Federal Institute of Technology Lausanne  
EPFL, IPEQ, 1015, Lausanne, Switzerland.

*dmitri.boiko@epfl.ch*

Active homostructure and heterostructure photonic crystals were realized using phased coupled arrays of vertical cavity surface emitting lasers (VCSELs), and their photonic modes were studied theoretically and experimentally.

**Keywords:** photonic crystals, VCSEL arrays, heterostructures

## Introduction

Phase-locked arrays of vertical cavity surface emitting lasers (VCSELs) represent a two-dimensional (2D) photonic crystal loaded with optical gain and loss. Both periodic [1] and quasi-periodic [2] VCSEL photonic crystals have been studied experimentally and theoretically. However, little progress has been made in understanding the polarization characteristics of [3] and the impact of a photonic heterostructure configuration on [4] the photonic modes in these structures.

In this paper, we introduce a model of equivalent 3D photonic crystal suitable for a standard method of analysis based on orthogonal plane waves (OPW) expansion [5]. The band structure and the supermode field pattern of rectangular-lattice photonic crystals are analyzed using this approach. The homostructure and heterostructure VCSEL photonic crystals are realized using electrically pumped InGaAs/AlGaAs devices emitting at 970 nm wavelength. The band structure and supermode patterns of these structures are measured and compared with our model.

## Model of Photonic States and Energy Bands

The 2D lateral periodicity of phase-locked VCSEL arrays is effectively introduced by patterning the reflectivity of the top distributed Bragg reflector (DBR) using higher-reflectivity metallic pixels separated by a lower-reflectivity grid [1]. The VCSEL cavity formed by the top and bottom DBRs results in an effective periodicity in the third direction, along the cavity axis ( $z$ -axis). Since the periodicity in reflectivity patterning enters through the boundary conditions, an equivalent, unfolded 3D photonic crystal is formed and can be analysed using an OPW expansion method.

The photonic modes are given by an electromagnetic Bloch wave propagating in the crystal with a periodically varying noninertiality given by

$$\mathbf{D} = \epsilon\mathbf{E} + [\mathbf{H} \times \mathbf{g}] \quad \mathbf{B} = \mu\mathbf{H} + [\mathbf{g} \times \mathbf{E}] \quad \mathbf{g} = -\hat{\mathbf{z}} \frac{ic}{\omega} \ln r(x, y) \sum_N \delta(z - 2NL) \quad (1)$$

where  $r(x, y)$  is the spatially modulated reflectivity with period  $\Lambda$ , and  $L$  is the cavity length. In a typical VCSELs array, the photonic mode propagates nearly parallel to the  $z$ -axis ( $|\mathbf{K}_\perp| \ll K_z$ ). In this case, the electric and magnetic field wave function  $|\mathbf{v}_{m\mathbf{k}}\rangle$  obeys the 2D Schrödinger equation

$$\left[ m_0 \left( \frac{c}{n} \right)^2 + \frac{\hat{\mathbf{p}}_\perp^2}{2m_0} + i \frac{c\hbar \ln(r(\mathbf{r}_\perp))}{n 2L} \right] |\mathbf{v}_{m\mathbf{k}}\rangle = \hbar\omega_{m\mathbf{k}} |\mathbf{v}_{m\mathbf{k}}\rangle, \quad m_0 = \frac{\hbar|K_z|n}{c} \quad (2)$$

where  $n$  is the refraction index in the cavity and  $\omega_{m\mathbf{k}}$  assume complex values. The analytic solution at the high symmetry points  $\Delta$ ,  $Z$  and  $T$  of the Brillouin zone (BZ) was obtained in the case of square symmetry of the reflectivity patterning [Fig. 1]. The intensity patterns of the main polarization components defined by the wave functions  $|\mathbf{v}_{m\mathbf{k}}\rangle$  are given in Fig. 2 [all states are

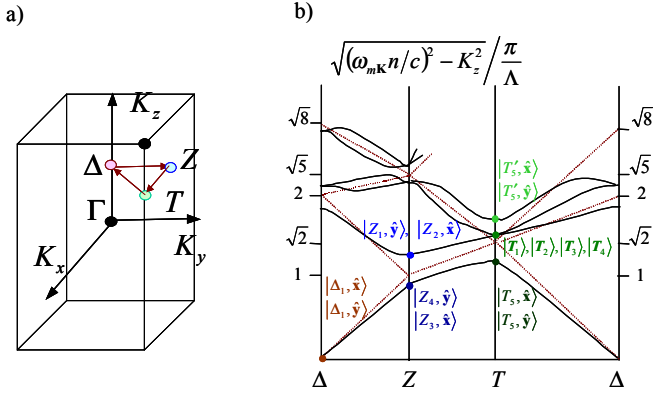


Fig.1. Brillouin zone of the photonic crystal (a); empty lattice test (dashed lines) and a simplified diagram of the energy bands (solid lines) (b).

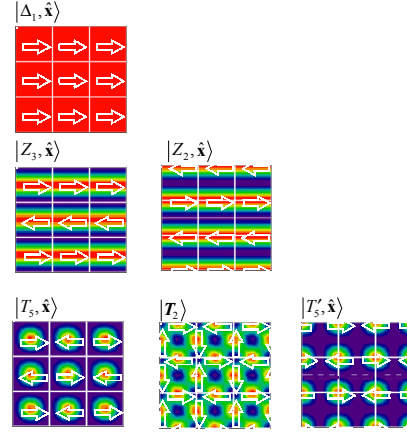


Fig 2: Calculated intensity patterns of the main polarization components at  $\Delta$ ,  $Z$ , and  $T$  points of BZ , arrows shows polarization.

doubly degenerate by polarization].

The  $T$  point [ $\mathbf{K} = (\frac{\pi}{\Lambda}, \frac{\pi}{\Lambda}, K_z)$ ] is of significant, practical interest [Fig.1.b], since the photonic state  $T_5$  has the lowest loss [Fig.3.a] and is the main lasing mode of the VCSEL array. This state is doubly degenerate by polarization and the electric field for  $|T_5, \hat{\mathbf{x}}\rangle$  and  $|T_5, \hat{\mathbf{y}}\rangle$  is given by

$$\begin{aligned} \hat{\mathbf{E}}|T_5, \hat{\mathbf{x}}\rangle &\propto \hat{\mathbf{x}} \cos \frac{\pi}{\Lambda} x \cos \frac{\pi}{\Lambda} y - \hat{\mathbf{z}} \frac{i\pi}{\Lambda K_z} \sin \frac{\pi}{\Lambda} x \cos \frac{\pi}{\Lambda} y + \hat{\mathbf{y}} \frac{\pi^2}{2\Lambda^2 K_z^2} \sin \frac{\pi}{\Lambda} x \sin \frac{\pi}{\Lambda} y \\ \hat{\mathbf{E}}|T_5, \hat{\mathbf{y}}\rangle &\propto \hat{\mathbf{y}} \cos \frac{\pi}{\Lambda} x \cos \frac{\pi}{\Lambda} y - \hat{\mathbf{z}} \frac{i\pi}{\Lambda K_z} \cos \frac{\pi}{\Lambda} x \sin \frac{\pi}{\Lambda} y + \hat{\mathbf{x}} \frac{\pi^2}{2\Lambda^2 K_z^2} \sin \frac{\pi}{\Lambda} x \sin \frac{\pi}{\Lambda} y \end{aligned} \quad (3)$$

It exhibits the anti-phase modulation at adjacent lattice sites and has intensity maxima (z-component of the Poynting vector) located at the high-reflectivity pixels. The intensity pattern is defined by the main polarization component since the z component of the field does not contribute to the energy flow along the z- axis, and  $\pi/\Lambda K_z \ll 1$ . This state is a hybrid mode ( $E_z, H_z \neq 0$ ) and has an orthogonal polarization component with intensity maxima located at the cross points of the array grid.

The full 2D transversal photonic band gap is opened if the photon energy in the  $|Z_2, \hat{\mathbf{x}}\rangle$  states is higher than for  $|T_5, \hat{\mathbf{x}}\rangle$ . The calculated photon energies are plotted in Fig.3. b [the phase difference  $\Delta\phi$  between the complex reflection coefficients at the pixel and at the grid is 0.1 rad]. The analysis

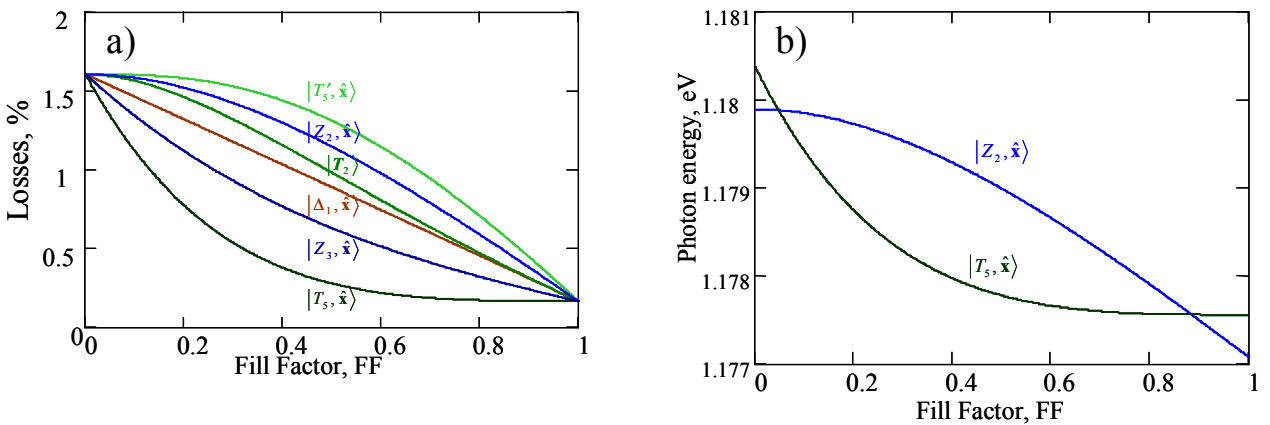


Fig.3. Losses of different modes (a) and photon energies in states  $|Z_2, \hat{\mathbf{x}}\rangle$  and  $|T_5, \hat{\mathbf{x}}\rangle$  (b) as a function of fill factor FF (ratio of the areas of the high-reflectivity pixel and of the unit cell)

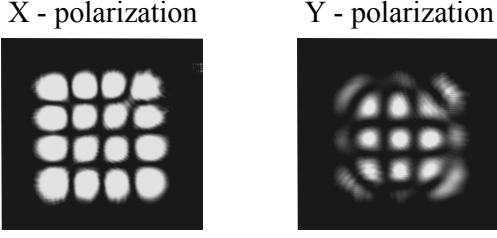


Fig.4 Measured polarization-resolved NF intensity pattern in  $|T_5, \hat{x}\rangle$  state of a CW lasing 4x4 VCSEL array.

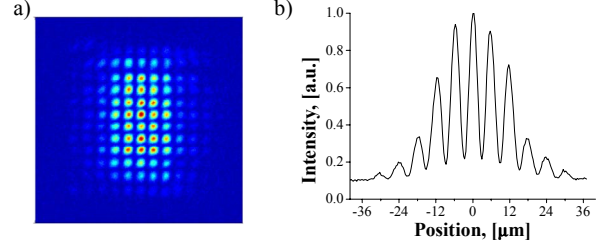


Fig.5. Measured near field intensity pattern (a) and near field cross section (b) of 16x16 VCSEL photonic heterostructure:  $\Lambda=6 \mu\text{m}$ ,  $FF_{core}=0.69$ ,  $FF_{clad}=0.34$ , core region contains 5x10 pixels.

reveals an optimal fill factor FF at which a minimal phase contrast  $\Delta\varphi$  is required to open this gap:

$$\frac{\Lambda^2 n}{\lambda L} > \frac{2.5}{\Delta\varphi} \quad \text{at} \quad FF_{opt} = 0.34 \quad (4)$$

### Measured Polarization-Resolved Mode Patterns

The measured polarization-resolved near field (NF) pattern of a 4x4 VCSELs array [Fig. 4] confirms the field distribution predicted by (3). It corresponds to the state  $|T_5, \hat{x}\rangle$ , with the main polarization component directed along the x- axis and with intensity maxima located at the VCSEL pixels ("pixel mode"). The weak y- polarized component of the field arises from the last term in (3). This component has intensity maxima located at the cross points of the array grid, which coincides with the intensity pattern of  $|T'_5, \hat{y}\rangle$  (and  $|T'_5, \hat{x}\rangle$ ) states ("grid cross mode"). Note that the detected polarization-resolved pattern in Fig.4 can be significantly influenced by the mixing of pixel mode states and of grid cross mode states due to the finite size of the array.

In fact, in arrays incorporating  $N \times N$  pixels, the state at the boundary of BZ cannot be realized because of the quantization of the transverse component of the wave vector  $\mathbf{K}$ . A simple analysis based on coupled mode theory shows that the mode closest to the T point of BZ is detuned by  $\mathbf{k}_\perp = \frac{\pi}{\Lambda} \left( \frac{-1}{N+1}, \frac{-1}{N+1} \right)$  from the T point. A  $\mathbf{k}_\perp \cdot \hat{\mathbf{p}}_\perp$  perturbation analysis of (2) demonstrates that for small energy gap  $\hbar\omega_{T'_5} - \hbar\omega_{T_5}$  values, the band mixing can enhance the amplitude of the complementary grid-type pattern.

### Realization and Analysis of Photonic Crystal Heterostructures

Photonic crystal heterostructures represent a hybridization of two (or more) periodic photonic crystals of different lattice and/or unit cell configurations [4]. The 2D photonic heterostructures studied here consist of a "core" region of larger pixel size VCSELs embedded in a "cladding" region of smaller size pixels. These heterostructures serve to confine the envelope function of the supermode to the vicinity of the large-pixel region. The envelope function exhibits a standing wave pattern in the core and decays exponentially in the cladding (see Fig. 5) [4].

The two regions of the heterostructure differ by the fill factor. This difference in the FF gives rise to a different dispersion, which induces the envelope function optical confinement. In the particular case of VCSELs photonic heterostructures, this confinement is related to the imaginary part of the dispersion curve  $\text{Im}(\omega_{m, \mathbf{k}_\perp})$ , which determines the VCSEL cavity loss. A  $\mathbf{k}_\perp \cdot \hat{\mathbf{p}}_\perp$  perturbation analysis of (2) yields the photon energy dispersion in the parabolic approximation:

$$\hbar\omega_{T_5 + \mathbf{k}_\perp} = \hbar\omega_{T_5} + \frac{\hbar^2 k_\perp^2}{2m^*}, \quad \frac{1}{m^*} = \frac{1}{m_0} - \frac{4}{m_0^2} \frac{P^2}{\hbar(\omega_{T_1} - \omega_{T_5})} \quad (5)$$

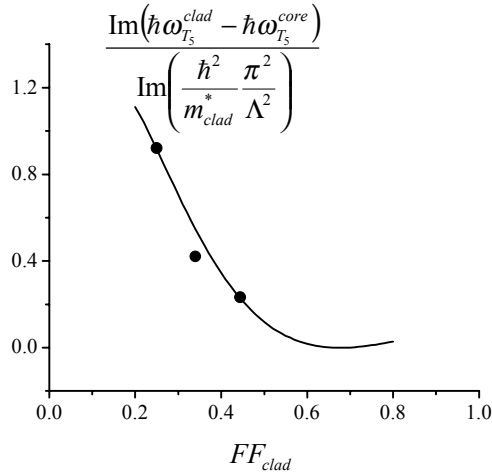


Fig. 6 Calculated (curve) and measured (points) relative band gap offset as a function of FF in the cladding,  $FF_{\text{core}} = 0.69$

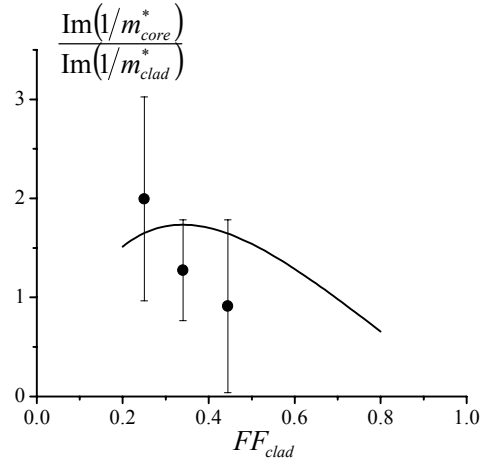


Fig.7 Calculated (curve) and measured (points) effective mass ratio as a function of FF of the cladding,  $FF_{\text{core}} = 0.69$ .

where  $P$  is the matrix element of the momentum operator. In the single band approximation, the parameters defining the confinement are the relative band offset at the band edge (see solid line in Fig 6) and the ratio of the effective masses (solid line in Fig.7).

In the experiment, these parameters were measured using a series of photonic heterostructure VCSELs with different array size and FF values. The FF of the core region was fixed at 0.69 while the one at the cladding was varied between 0.25 and 0.44. The fit of the measured near field envelope function has allowed to deduce the propagation constants in the core and cladding regions. To evaluate the relative band edge offset and effective mass, two points on the dispersion curve are required (in the parabolic approximation). To access different values of the transverse wave vector near the band edge, the intensity patterns of arrays with different number of pixels along the  $x$ -axis (with fixed values of the FF in the core and the cladding) were evaluated. Reasonable agreement with the calculated values was obtained (see symbols in Figs. 6 and 7). The discrepancy of measured and calculated ratio of effective mass can be partly explained by the finite size (up to 16X16 pixels) of the measured arrays.

## Conclusion

Coherent VCSELs arrays provide an efficient configuration for manipulating the polarization state and the intensity patterns of lasing photonic modes. In particular, the realization of photonic crystal heterostructures yields a new approach for achieving confinement of the envelope functions of photonic modes. We have developed a model for analyzing the polarization modes in 2D photonic crystal consisting of coupled VCSELs. The similarity of the method to the formalism of solid-state physics of electronic crystals allows the  $\mathbf{k} \cdot \hat{\mathbf{p}}$  perturbation method to be applied for the analysis of the dispersion, and the effective mass Hamiltonian is applicable for the analysis of the photon confinement in photonic heterostructures. The results of the analysis are in good agreement with our experimental observation.

- [1] M. Orenstein, E. Kapon, N.G. Stoffel et al., *Appl. Phys. Lett.* **58**, 804-806,1991.
- [2] H. Pier, E. Kapon and M. Moser, *Nature* **407**, 880-883, 2000.
- [3] P. Debernardi, G.P. Bava, F. Monti di Sopra and M.B. Willemsen, *IEEE J. Quantum Electron.* **39**, 1-12, 2003.
- [4] C.-A. Berseth, G. Guerrero, E. Kapon et al., *Proc. CLEO 2000*, pp 171-172, CtuA48, 2000.
- [5] K.M. Leung, Y.F. Liu, *Phys. Rev.B* **41** , 10 188- 10 190, 1990